Uniaxial magnetic anisotropy in Pd/Fe bilayers on Al2O3 (0001) induced by oblique deposition

Chiao-Sung Chi, Bo-Yao Wang, Way-Faung Pong, Tsung-Ying Ho, Cheng-Jui Tsai, Fang-Yuh Lo, Ming-Yau Chern, and Wen-Chin Lin

Citation: Journal of Applied Physics **111**, 123918 (2012); doi: 10.1063/1.4730632
View online: http://dx.doi.org/10.1063/1.4730632
View Table of Contents: http://scitation.aip.org/content/aip/journal/jap/111/12?ver=pdfcov
Published by the AIP Publishing

Uniaxial magnetic anisotropy in Pd/Fe bilayers on Al_2O_3 (0001) induced by oblique deposition

Chiao-Sung Chi,[1] Bo-Yao Wang,[2] Way-Faung Pong,[2] Tsung-Ying Ho,[1] Cheng-Jui Tsai,[1] Fang-Yuh Lo,[1] Ming-Yau Chern,[3] and Wen-Chin Lin[1,a)]
[1]*Department of Physics, National Taiwan Normal University, 116 Taipei, Taiwan*
[2]*Department of Physics, Tamkang University, Tamsui 251, Taiwan*
[3]*Department of Physics, National Taiwan University, 106 Taipei, Taiwan*

(Received 27 February 2012; accepted 22 May 2012; published online 27 June 2012)

This study reports the preparation of self-organized 1-dimensional magnetic structures of Fe on Al_2O_3 (0001) by oblique deposition. The x-ray diffraction (XRD) results in this study show the preferred (110) texture of the Fe films. XRD and extended x-ray adsorption fine structure measurements indicate larger oblique deposition angle (65°) leads to more disorder in the Fe crystalline structure. After capping with a Pd overlayer, the Pd/Fe/Al_2O_3 (0001) still exhibits uniaxial magnetic anisotropy induced by the underlying 1-dimensional Fe nanostructure. This uniaxial magnetic anisotropy changes with the variation in Fe thickness and oblique deposition angle. These results clearly indicate the feasibility of manipulating uniaxial magnetic anisotropy and crystalline order through the oblique deposition of magnetic materials. © *2012 American Institute of Physics*. [http://dx.doi.org/10.1063/1.4730632]

I. INTRODUCTION

The magnetic anisotropy energy (MAE) of ferromagnetic (FM) materials can be defined as the energy difference between the different orientations of the magnetic moment. The MAE not only determines the easy magnetization direction and the stability of the ferromagnetic ordering (i.e., Curie temperature) but also correlated to the magnetization processes of FM materials.[1,2] Because of the physical origins of the MAE, the manipulation of MAE has been demonstrated. It is feasible to manipulate the MAE, especially in nano-scale materials, for applications in magnetic data storages and nano-devices. One of the practical methods of tuning MAE is to change the shape of the magnetic materials (i.e., shape magnetic anisotropy). Self-organized approaches are promising methods of fabricating nano-structured thin films and controlling the shape-induced MAE.[3–5] Because of shadowing and steering effects, the oblique deposition of magnetic atoms on suitable substrates can lead to highly elongated grains or ripples on nanometer scale.[6–15] These elongated nanograins or ripples induce a uniaxial MAE.[11,16] This method of manipulating MAE is easy to apply to magnetic nano-devices. Most previous studies on this topic have focused on the oblique-incidence epitaxial growth on metal(001), for example Co/Cu(001) and Fe/Ag(001).[6,7] Recent studies have extended this approach to the heterostructures of metal/semicondutor and metal/insulator, such as Fe/MgO(001) and Co/Si(111).[10–14] For cubic (001) substrates, the oblique-deposition induced uniaxial MAE usually mixes with a four-fold symmetric MAE, which originates from the substrate crystalline structure. In the sixfold symmetric case, the substrate-induced crystalline MAE is relatively weak, and the grazing-incidence growth effect on the MAE is easy to examine and control.[11] Until now, the oblique deposition-induced uniaxial MAE has been limited to only a few substrates, and some crucial issues remain unclear. For example, will a protective capping layer destroy the self-organized nanostructure and the uniaxial MAE? Few studies have discussed capping layer effect, which is unavoidable in application. How does the crystalline structure evolve with an increasing oblique angle? The change in crystalline ordering as a function of oblique angle is crucial to magnetic behavior because the crystalline MAE are changed in the grazing-incidence grown films. In this study, Fe films were grown on single crystalline sapphire Al_2O_3 (0001) substrates by oblique-incidence deposition. The Fe films were covered by a normally deposited Pd layer. The transparency of Al_2O_3 substrate makes this system as a suitable candidate for controlling optical transmission in magneto-optical plasmonic applications.[17] A Pd capping layer was added to protect the FM layer and to allow future study of H_2-absorption effect on magneto-optical properties.[18] This study investigates the changes in surface morphology, crystalline structure, and magnetic behavior caused by oblique deposition.

II. EXPERIMENT

The sample was prepared in a vacuum chamber with a base pressure of 3×10^{-9} Torr. Single crystalline sapphire Al_2O_3 (0001) ($3 \times 5 \times 0.33$ mm) was used as the substrate. After cleaning with 95% ethyl alcohol, Al_2O_3 (0001) substrates were annealed at 400 K for 12 h in vacuum. The Pd/Fe bilayers were grown at room temperature (RT) by e-beam heated thermal evaporation. Fe films were deposited on Al_2O_3 (0001) with a variation of thickness (10-150 monolayers) and deposition angles (0°, 45°, and 65° to the surface normal of the substrate). The Pd capping layer was then deposited in the surface normal direction on top of Fe for

a)E-mail: wclin@ntnu.edu.tw.

protection. Unless otherwise mentioned, the Pd thickness was fixed at 40 monolayers (ML). The Fe and Pd atoms were evaporated by e-beam heating. The deposition rate was calibrated from the epitaxial growth on Cu(100) using Auger electron spectroscopy. Thus, 1 ML is equivalent to the nominal surface atom density of 1.54×10^{15} atoms/cm^2. The corresponding magnetic hysteresis loops were measured by the magneto optical Kerr effect (MOKE) with azimuthal rotation to measure the oblique deposition-induced uniaxial anisotropy. The crystalline structure was characterized by x-ray diffraction (XRD) and extended x-ray absorption fine structure (EXAFS).[19–22] For XRD measurements, a Cu target was used to obtain the Bragg reflections from the samples. The atomic structure of Fe was measured by Fe *K*-edge EXAFS using total fluorescence yield (TFY) at the BL16A beamline at the National Synchrotron Radiation Research Center (NSRRC) in Hsinchu Taiwan. The surface morphology of Pd/Fe/Al_2O_3 (0001) was *exsitu* characterized using scanning tunneling microscope (STM).

III. RESULT AND DISCUSSION

A. Morphology

Previous studies have shown that the shadowing and steering effects induced by oblique deposition significantly increase the roughness of the grown film.[8] The surface morphology exhibits highly elongated grains or ripples on the nanometer scale. For example, pulsed laser off-normal deposited Co films have a nano-string structure measuring 8 to 20 nm wide and 120 nm long.[15] Bubendorff *et al.* presented a STM investigation on Fe/Si(111) showing that as the incidence angle increases, the surface islands elongate in the direction perpendicular to the incident atomic flux, leading to the formation of a ripple structure.[14] Because the Al_2O_3 (0001) substrate is an insulator, the electron tunneling works well only when the Fe atoms form a continuous film on Al_2O_3 (0001). In other words, when the surface still consists of discrete 1D Fe nano-stripes, the conducting property prevents STM investigation. This study focuses on the magnetic properties of Pd-covered Fe/Al_2O_3 (0001), rather than the uncovered Fe/Al_2O_3 (0001). Because oblique deposition-induced 1-dimensional ripples have been previously reported in several systems,[11–16] this study investigates the capping layer effect, which is unavoidable in application, and seldom discussed in previous reports. How is the surface morphology affected after adding a capping layer? Does a capping layer destroy the grazing incidence grown 1D nanostructures, and the induced uniaxial anisotropy? Fig. 1 shows STM images of Pd/Fe bilayers grown on Al_2O_3 (0001) with different Fe oblique deposition angles: 0°, 45°, and 65°. The oblique angle is defined as the angle between the surface normal and grazing incidence direction. Thus, 0°-Fe means the Fe film is deposited from the surface normal direction. The STM images reveal the surface morphology of the Pd capping layer on the obliquely deposited Fe films. Because the Pd layer was deposited in the surface normal direction, it is interesting to know if the Fe oblique deposition-induced 1-dimensional nanostructures are still observable after capping procedure. In Fig. 1(a), the morphology of Pd on 0°-Fe consists of nanostripes. Each stripe is 5 ± 2 nm wide, and the length ranges in several tens of nanometers. The surface corrugation is within ± 3 nm. In the magnified STM image, the orientations of the stripes clearly reveal a three-fold symmetry that might originate from the hexagonal crystalline structure of the substrate Al_2O_3 (0001). In Figs. 1(b) and 1(c), the morphology of 40 ML Pd on 70 ML 45° and 65°-deposited Fe consists of randomly distributed clusters. The average cluster size is 10 ± 3 nm, and the surface roughness is within ± 5 nm. A comparison of Figs. 1(a)–1(c) shows that the 40 ML Pd capping layer fully covered the 1-dimensional Fe nanostructures for the cases of 45° and 65°-Fe. However, the Pd capping layer can still preserve the 3-fold symmetry of the 0°-Fe/Al_2O_3 (0001) films.

Fig. 1(d) shows another example of the Pd/45°-Fe bilayer, in which the Pd capping layer is much thinner than those shown in Figs. 1(a)–1(c). The surface morphology consists of nano-sized clusters, like Fig. 1(b), but with a much smaller average size ($\approx 5 \pm 2$ nm) and a smaller surface corrugation ($\leq \pm 2$ nm). A comparison between Figs. 1(b) and 1(d) shows that the thicker the Pd coverage is, the larger the Pd surface nanoclusters are.

B. Crystalline structure

To characterize the crystalline structure, an x-ray diffractometer with a Cu target was used to obtain the Bragg reflections from the samples. Fig. 2 shows the x-ray diffraction patterns of three Pd/100 ML Fe bilayer films on Al_2O_3 (0001). The Fe films were deposited with oblique angles of 0°, 45°, and 65°. Cu-K α x-rays contribute the large main peak of Al_2O_3 (0006) at $2\theta \approx 41.6°$, confirming the highly oriented crystalline structure of the sapphire substrate.[23]

As indicated by the arrows, the peaks of Fe(110) and Fe(200) appear at $2\theta \approx 44.6°$ and $2\theta \approx 64.4°$, respectively.[24,25] For 0°-Fe, the Fe(110) peak is especially pronounced and much larger than the Fe(200) peak, indicating the body-centered-cubic (110) is the preferred orientation for normally deposited Fe on Al_2O_3 (0001). For 45°-Fe, the peaks of Fe(110) and Fe(200) are still observable and of similar intensity, suggesting the coexistence of both orientations. For 65°-Fe, only the peak of Fe(110) is apparent. This also shows the preference for bcc(110) orientation in 65°-Fe. These observations lead to two conclusions. First, the (110) orientation is preferred in the Fe films grown on Al_2O_3 (0001), especially for 0° and 65°-Fe. Second, the off-normal 65° grazing incidence growth causes the disappearance of the (100) texture of Fe. Roughly speaking, the grazing-incidence growth leads to less pronounced XRD peaks of Fe (i.e., more disordering in the crystalline structure). The peak of Pd(111) appears at $2\theta \approx 40.0°$, showing the preference for Pd(111) texture in the Pd polycrystalline layer.[26]

The combination of metals with oxide substrates is critically important to understanding various phenomena related to composite materials and heterogeneous catalysts. Many experimental and theoretical studies have recently focused on the Al_2O_3 (0001) surface. The literature shows that the most stable (0001) surface of Al_2O_3 is terminated by a single Al layer. This surface undergoes large relaxation, where the

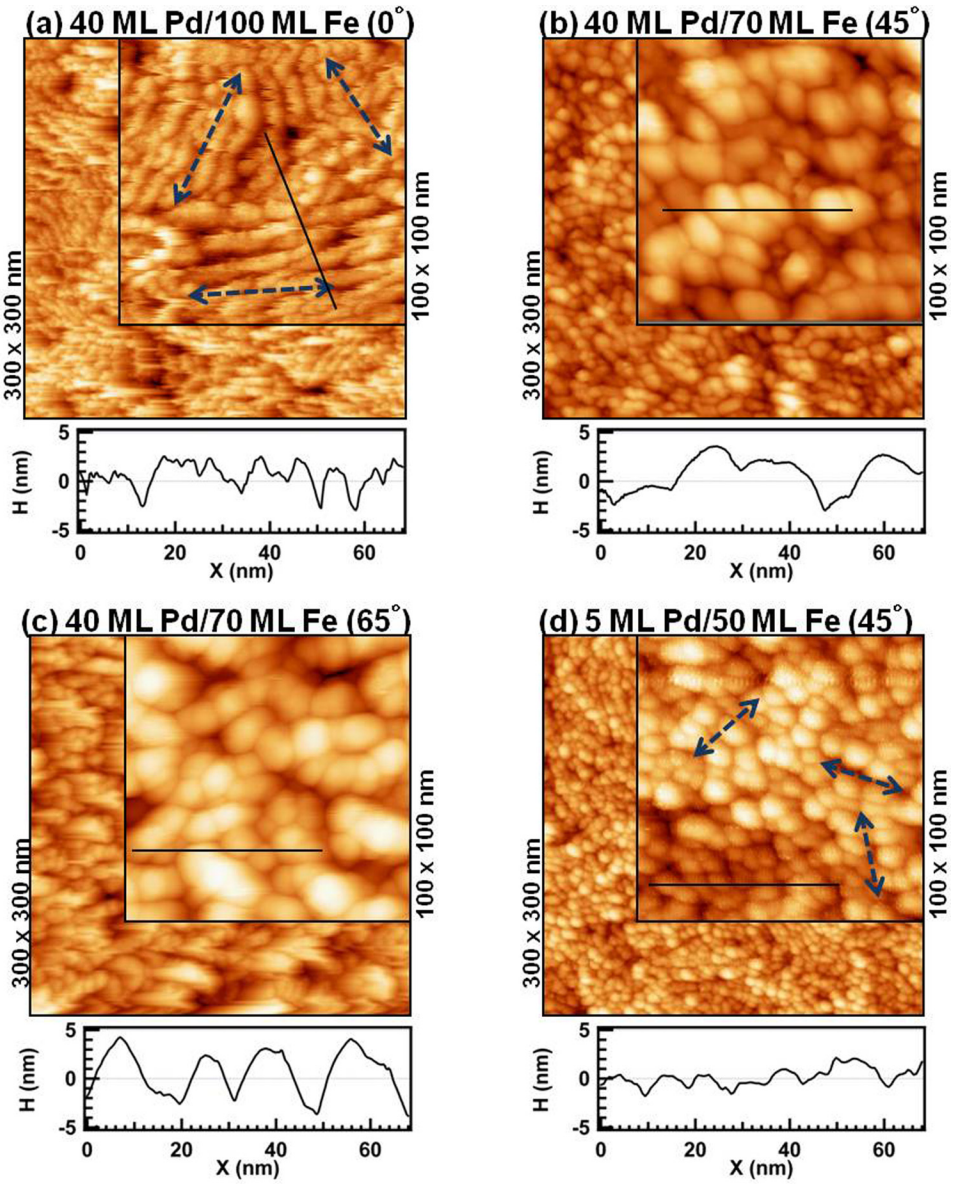

FIG. 1. STM images of Pd/0°, 45°, and 65°-deposited Fe films on Al_2O_3 (0001).

surface aluminum moves into the bulk, ending up almost coplanar with the oxygen.[27] Fig. 2(b) shows a top-down view of the crystalline structures of Al_2O_3 (0001) and bcc Fe(110). The open circles and gray circles indicate the first layer of aluminum and oxygen atoms, respectively.[28,29] Because of the surface relaxations, the oxygen atoms cannot form a perfect hexagonal structure. Instead, the surface atomic structure of oxygen consists of a rectangular and a parallelogram lattice cell, as indicated in the upper panel of Fig. 2(b). The Fe(110) surface crystalline also consists of a rectangular lattice cell. Although the lattice mismatch in the long edge direction is much larger, approximately 17%, the ratio of the two lattice lengths is close to the ratio of the two integers 6/5. This means 5 cells of Al_2O_3 (0001) can match 6 cells of Fe(110) well. The crystalline structures of Fe(110) in Fig. 2(b) does not perfectly match Al_2O_3 (0001). However, because of the similar lattice structure, it is reasonable to expect some short range ordered Fe(110) structures on Al_2O_3 (0001). Research by Dedkov *et al*. regarding epitaxial Al_2O_3 (0001) layers on Fe(110) also supports this suggestion.[28] The lower panel of Fig. 2(b) shows the three possible orientations of Fe(110) grown on the Al_2O_3 (0001) surface, which is consistent with the 3-fold symmetry observed in Fig. 1(a).[30]

In addition to the crystalline characterization by XRD, this study uses EXAFS measurement to determine the local atomic geometry of obliquely deposited Fe.[19,21] Fig. 3(a) shows the k^2-weighted Fe *K*-edge EXAFS oscillation. The EXAFS spectra in this figure were recorded at room temperature at normal incidence with the polarization parallel to the 1-dimensional Fe ripples. Fig. 3(b) represents the Fe *K*-edge Fourier transform (FT) amplitudes of the EXAFS $k^2\chi$ data for the Fe films. For the oblique deposition angles of 0°, 45°, and 65°, the first peaks in the FT spectra appear to have roughly the same location, though they have different heights and full widths at the half maximum. In addition to the normal incidence geometry with polarization parallel to the Fe ripples (Fig. 3), this study includes EXAFS measurements with other geometry. One is "grazing incidence along the ripple direction + polarization parallel to the surface normal," and the other one is "normal incidence + polarization

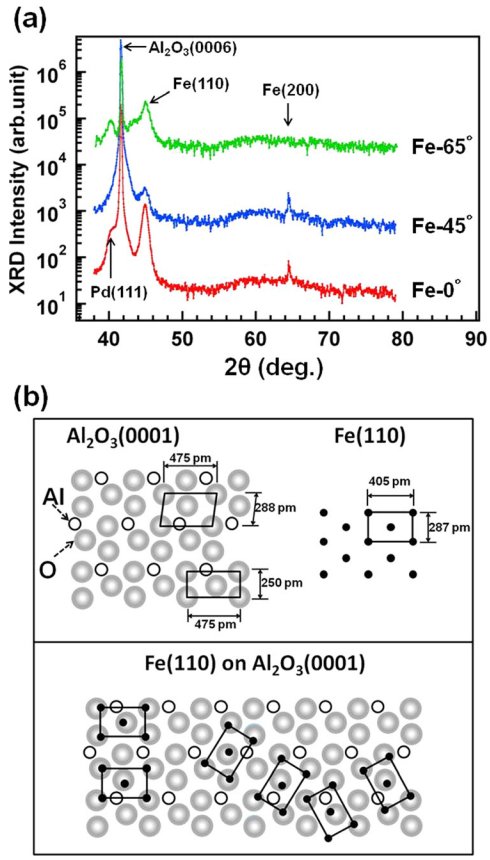

FIG. 2. (a) X-ray diffraction patterns of Pd/100 ML Fe bilayer films on Al_2O_3 (0001). (b)Upper panel: top view of the crystalline structure of Al_2O_3 (0001) and Fe(110) surface. For Al_2O_3 (0001), the open circles and gray circles indicate the first layer of Al and O atoms, respectively.[28,29] Lower panel: the three possible orientations of Fe(110) grown on Al_2O_3 (0001).

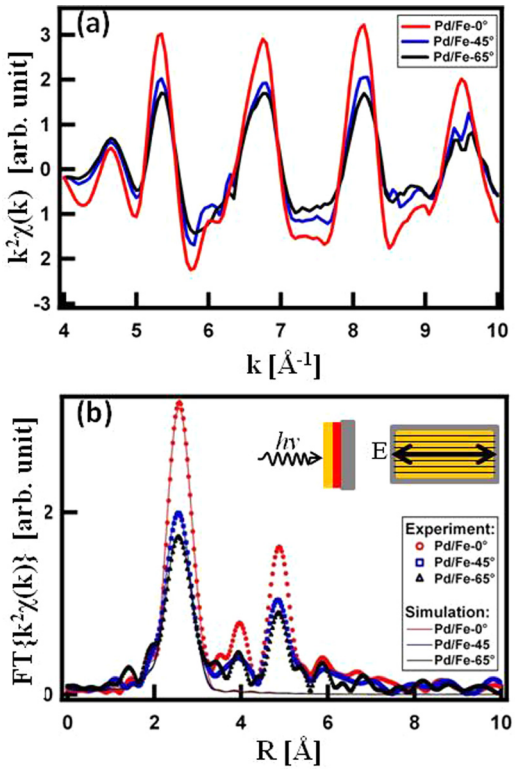

FIG. 3. (a) The EXAFS $k^2\chi$ (k) data and (b) the Fourier transform amplitudes of $k^2\chi$ (*k*) at the Fe *K*-edge for Pd/100 ML 0°-Fe, 70 ML 45°-Fe, and 70 ML 65°-Fe bilayers on Al_2O_3 (0001).

perpendicular to the Fe ripples." These measurements show similar results to Fig. 3(b). The first FT peak positions are invariant, but the peak height significantly decreases as the oblique deposition angle increases. This also suggests that the local crystalline structure of Fe becomes more disordered, when the Fe layer is deposited with a larger oblique angle.

Obtaining quantitative information about the local atomic structures near Fe atoms in the Pd/Fe/Al_2O_3 requires the analysis using the UWXAFS code, which involves the combination of a multiple-scattering EXAFS computer program, FEFF (Ref. 31) and a nonlinear least-square-fitting computer program, FEFFIT.[32] The fitting results appear in Fig. 3(b). The coordinating number of Fe was fixed at 8 when fitting to the experimental EXAFS. This fitting makes it possible to deduce the nearest neighbor (NN) distance surrounding Fe (R) and the mean square relative displacement (σ^2) for each NN bound, as listed in Table I. For the different oblique angles, the nearest neighbor distance for Fe (R) is nearly the same: $\approx 2.46 \pm 0.01$ Å, consistent with the body-centered-cubic Fe structure. However, the σ^2 significantly increases with the oblique growth angle, from 8.9 ± 0.5 ($\times 10^{-3}$ Å^2) for 0° to 14.5 ± 0.5 ($\times 10^{-3}$ Å^2) for 65°. Apparently, a large oblique deposition angle induces the 1-dimensional Fe surface nanostructures and leads to the disordering of crystalline structures. The stacking of grazing-incident atoms becomes more random as the oblique angle increases, leading to a larger variation in the mean square relative displacement (σ^2) for each NN bound.

C. Magnetic property

Fig. 4 shows the azimuthal angle (ϕ)-dependent MOKE hysteresis loops of Pd/25 ML 0°, 45°, 65°-deposited Fe/Al_2O_3 (0001). For Pd/0°-deposited Fe/Al_2O_3 (0001), the hysteresis loops have a square shape and are nearly invariant in ϕ. This invariance implies the weak in-plane magnetic anisotropy and indicates the absence of the uniaxial magnetic anisotropy. For 45° deposition, the sample shows a square loop when ϕ is close to 0°. When ϕ approaches 90°, it means the magnetic field (H) is perpendicular to the 1-dimensional ripples of Fe, the hysteresis loops gradually become tilted and the remanence decreases to almost zero. The ϕ -dependent evolution of MOKE hysteresis loops suggests the presence of uniaxial magnetic anisotropy induced by oblique deposition. The magnetic easy axis is in the $\phi = 0°$ direction,

TABLE I. Nearest neighbor distance around Fe (R) and the mean square relative displacement (σ^2) for each NN bound deduced from EXAFS.

Oblique Angle	R (Å) ± 0.01	σ^2 (Å^2) ± 0.5 × 10^{-3}
0°-Fe	2.47	8.9×10^{-3}
45°-Fe	2.46	13.1×10^{-3}
65°-Fe	2.46	14.5×10^{-3}

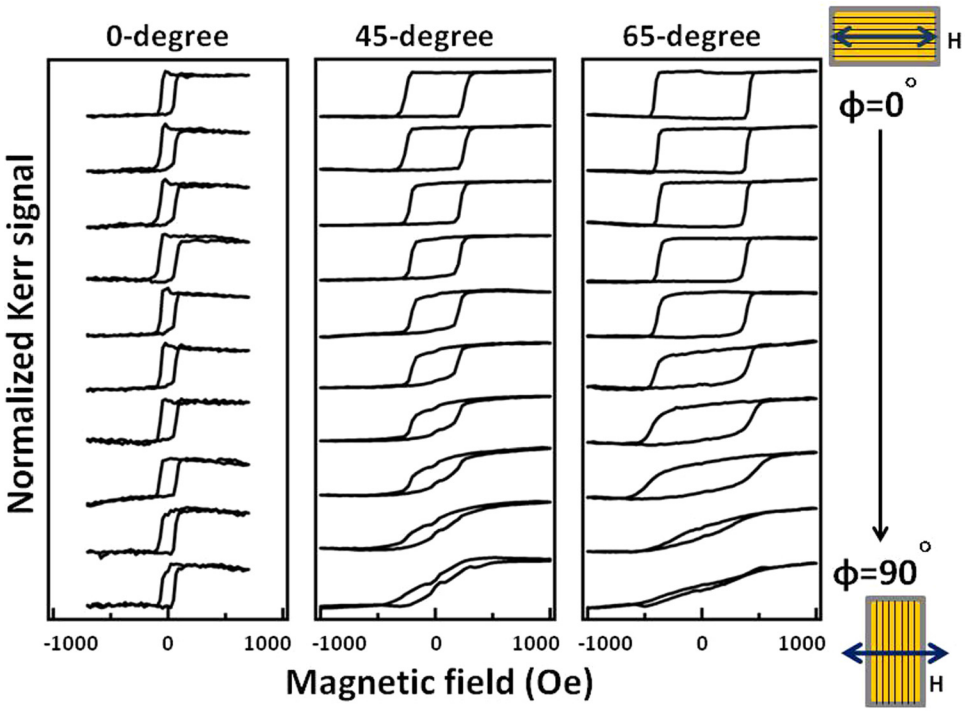

FIG. 4. MOKE hysteresis loops of Pd/25 ML 0°, 45°, 65°-deposited Fe/Al_2O_3 (0001), measured with the variation in azimuthal angle ϕ in a step of 10°. $\phi = 0°$ corresponds to the condition of parallel alignment of the magnetic field and Fe surface ripples.

which is parallel to the 1-dimensional ripples of Fe, while the magnetic hard axis is in the $\phi = 90°$ direction, which is perpendicular to the Fe ripples. Pd/65°-deposited Fe/Al_2O_3 (0001) exhibits uniaxial anisotropy similar to Pd/45°-Fe, but with a larger coercivity field (H_C) in the easy axis measurement and a larger saturation field (H_S) in the hard axis measurement.

For each oblique deposition angle (0°, 45°, and 65°), a series of Pd/Fe bilayers was prepared with the variation in Fe thickness. Fig. 5 presents a summary of the azimuthal angle ϕ-dependent MOKE measurement. The ratio of remanence (M_R) to saturation (M_S), and coercivity field (H_C) are plotted as a function of ϕ. In Figs. 5(a) and 5(d), 25–60 ML of 0°-Fe causes the isotropic magnetic behavior. The coercivity (H_C) ranges between 80 and 100 Oe and is invariant with azimuthal ϕ. The ratio of M_R/M_S is always close to 1, expressing the squareness of the hysteresis loops.

When the oblique deposition angle increases to 45°, as shown in Fig. 5(b), the H_C measured along the easy axis gradually increases from 100 Oe to 380 Oe, as the Fe thickness increases from 10 ML to 68 ML. Similar to Fig. 4, for each sample of 45°-Fe, the hysteresis loop gradually becomes tilted with increasing azimuthal ϕ. The H_C does not change seriously, until $\phi = 70°$. Because of the tilting shape of the hysteresis loop, H_C drops to almost zero in the hard axis ($\phi = 90°$). Unlike the insignificant change in H_C during $\phi = 0°$-70°, the ratio of M_r/M_S starts to decrease immediately after deviating from the easy axis ($\phi = 0°$). In the hard axis ($\phi = 90°$), M_r drops to nearly zero, indicating that no magnetic moment can be stabilized in that direction without the support of external magnetic field.

For Pd/65°-Fe/Al_2O_3 (0001), similar to the case of 45°-Fe, the drop of H_C and M_r/M_S ratio to the minimum at ($\phi = 90°$) clearly indicates the presence of uniaxial anisotropy. As shown in Figs. 5(c) and 5(f), both the H_C and the M_r/M_S ratio of Pd/20 ML 65°-Fe decreases more quickly with ϕ rotation than the other samples do. This implies the uniqueness of 65°-Fe in the thickness region close to 20 ML. The phase diagram in Fig. 6(a) also shows the distinctive evolution of H_C displayed by 65°-Fe. The coercivity (H_C) of 65°-Fe gradually increases with Fe film thickness and reaches the maximum H_C of 450 Oe at 20–40 ML. The H_C gradually decreases to approximately 300 Oe and becomes nearly invariant. A similar tendency of thickness-dependent H_C evolution appears in other systems.[16] The increase and subsequent decrease of H_C as a function of Fe film thickness might be related to the formation of 1-dimensional ripples. Before 20 ML, the ripples become steeper as the Fe thickness increases. With a higher coverage of more than 40 ML, the Fe ripples start to merge with their nearest neighbors, causing the decrease and saturation of H_C.[14,16] On the other hand, the coercivity of 45°-Fe monotonously increases with Fe film thickness and gradually becomes saturated at $H_C \sim 350$ Oe after 60 ML. In the case of 0°-Fe, the H_C ranges between 60 and 80 Oe and is nearly invariant with the changes in the Fe film thickness.

In addition to the Pd/0°, 45°, 65°-Fe bilayers, this study investigates the magnetic properties of Pd/45°-Fe/Pd trilayers for comparison. For the trilayers, both the bottom and top layer of Pd were deposited in the surface normal direction. The thickness-dependent evolution of H_C appears in Fig. 6(a), as indicated by the open squares. Interestingly, inserting a Pd buffer layer between the 45°-deposited Fe layer and Al_2O_3 (0001) destroys the uniaxial MAE, leading to a relatively small value of $H_C \approx 70 \pm 10$ Oe, which is similar to the H_C of Pd/0°-Fe bilayers. This implies the oblique deposition of Fe can induce a uniaxial MAE on a smooth and clean Al_2O_3 (0001) surface. The presence of a Pd buffer layer may already generate a relative rough surface because of the Volmer Weber (VW) growth, which can destroy the

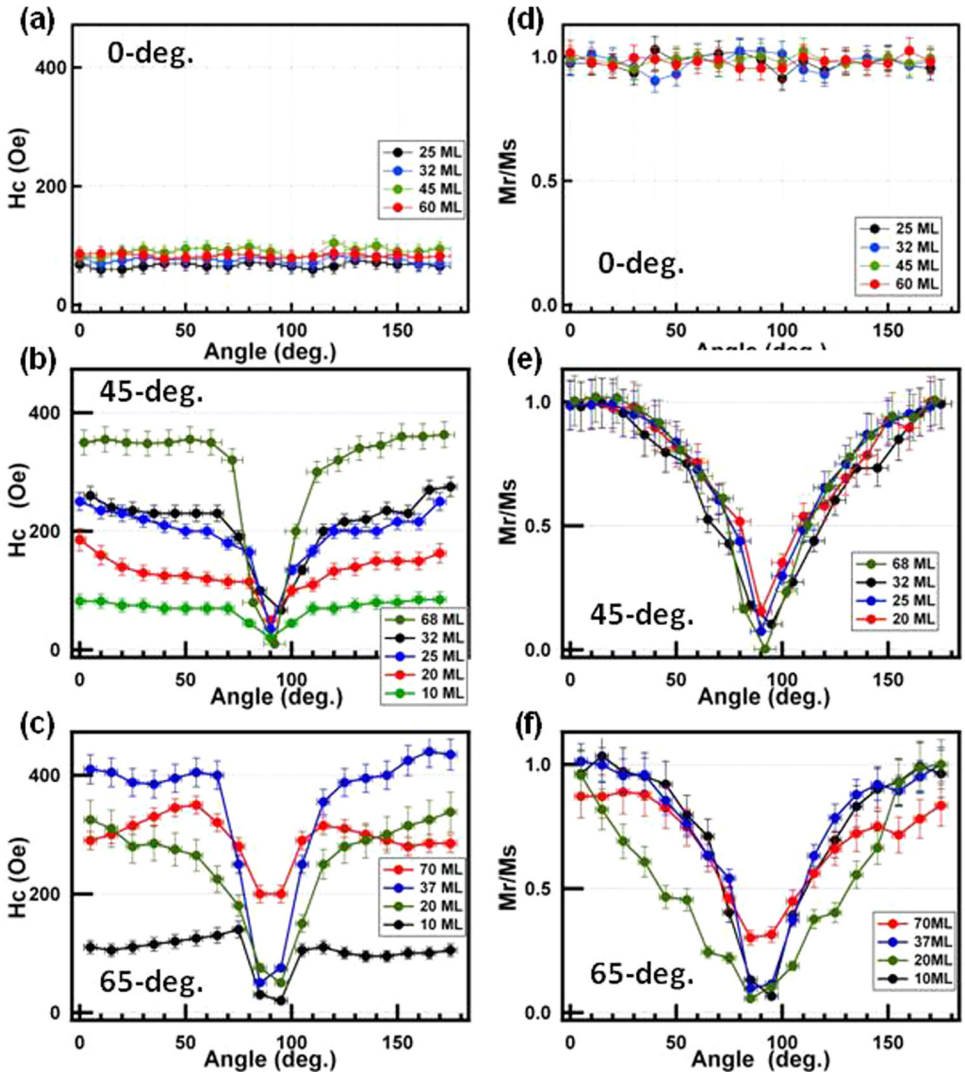

FIG. 5. Magnetic coercivity (H_c) and normalized remanence (M_r/M_s) for Pd/0°, 45°, 65°-deposited Fe/Al_2O_3 (0001), plotted as a function of azimuthal angle ϕ.

shadowing effect during the grazing-incidence growth of Fe, as well as the induced uniaxial MAE.[33]

Fig. 6(b) shows a summarized phase diagram of saturation field (H_S) measured in the hard axis (left axis), and the corresponding uniaxial MAE (right axis). By neglecting the crystalline MAE in Néel's model of surface anisotropy,[16] the uniaxial MAE (K_u) can be deduced from the H_S: $K_u = H_S$ M/2, where M is the magnetic moment of Fe (2.5 μ_B/atom). According to previous studies, both the crystalline MAE and shape-induced uniaxial MAE should be considered in the magnetization process.[10,34,35] The hysteresis loops in Fig. 4 show two-step-like loops when the angle is close to 90°, because there is always a kink (discontinuity in slope) at H = 0. Previous studies show that the coexistence of biaxial and uniaxial magnetic anisotropy can produce very clear two-step hysteresis loops, in which the minor loops are well-separated and the shift field can be quantitatively measured.[10,36,37] However, in the experimental results of Fig. 4, the two-step switching behavior is rather unclear, especially for quantitative determination of the shift field. Previous research reports clear 2-step loops in Fe/Ag(001), Co/Cu(001), Fe/MgO(001), and others.[10,36,37] All of them are epitaxial magnetic thin films on a four-fold symmetric substrate. In these systems, because of the single crystalline atomic structure, the biaxial magnetocrystalline anisotropy is well-defined and plays an important role in 2-step loops. For Fe/Al_2O_3 (0001), however, the randomly oriented nucleation grains in the Fe film and the 6-fold symmetry of the substrate significantly weakened the crystalline anisotropy. Therefore, the oblique-deposition induced uniaxial magnetic anisotropy dominates the magnetization process, generating indistinct two-step loops when the angle is close to 90°. Similar results were also reported on a Co/Si(111) system, in which a relatively weak intrinsic magnetocrystalline anisotropy is observed in additional to the dominant uniaxial magnetic anisotropy, and no clear 2-step loops were observed in the hard-axis measurement.[11] Because of the randomly oriented nucleation grains in the thin films and the 6-fold symmetry of the substrate, the intrinsic magnetocrystalline anisotropy of Fe/Al_2O_3 (0001) films is relatively weak, and the magnetization behavior is dominated by the uniaxial magnetic anisotropy. Thus, for the first step of estimation, the magnetocrystalline magnetic anisotropy should be negligible. The bulk crystalline MAE of bulk Fe (3.4 μeV/atom)[25] is of the same order of magnitude as the uniaxial MAE shown in Fig. 6(b). However, as measured by EXAFS and shown in Fig. 3, the disorder in the crystalline structure of the grazing-incidence grown Fe films randomizes the orientation of the

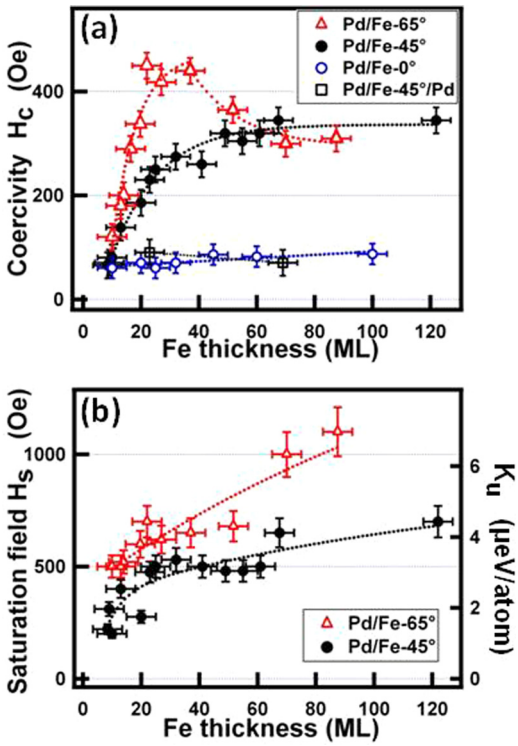

FIG. 6. Summarized (a) magnetic coercivity (H_c) measured in the easy direction, (b) saturation field (H_s) measured in the hard direction and the deduced uniaxial anisotropy (k_u) for Pd/Fe/Al_2O_3 (0001) with the variation in oblique deposition angle and thickness of the Fe layer. The dotted lines are guides for the eye.

crystalline MAE and thus reduces its total contribution. Eventually the shape induced uniaxial MAE dominates the magnetic behavior of the Pd/Fe bilayers.

IV. SUMMARY

This study investigates the surface morphology, crystalline structure, and magnetic behavior of Pd/obliquely deposited Fe/Al_2O_3. The Fe films on Al_2O_3 (0001) prefer the bcc(110) texture, whereas the Pd capping layer prefers the (111) orientation. The gazing-incidence growth of the Fe layer induces a uniaxial magnetic anisotropy (MAE). The magnetic easy direction is on the surface plane and perpendicular to the grazing-incidence direction. This uniaxial MAE increases with the Fe film thickness and oblique deposition angle. The higher the oblique deposition angle results in a larger coercivity, a larger uniaxial MAE, and more obvious disordering in the crystalline structure. The detailed correlations between morphology, crystalline structure, and MAE shown in this report will be valuable to future research and applications.

ACKNOWLEDGMENTS

This work was supported by the National Science Council of Taiwan under Grant Nos. NSC 99-2738-M-003-001, NSC 99-2112-M-003-009-MY3, and NSC 99-2923-M-003-001-MY2.

[1]S. Cherifi, R. Hertel, A. Locatelli, Y. Watanable, G. Potdevin, A. Ballestrazzi, M. Balboni, and S. Heun, Appl. Phys. Lett. **91**, 92502 (2007).
[2]C. C. Kuo, C. L. Chiu, W. C. Lin, and M.-T. Lin, Surf. Sci. **520**, 121 (2002).
[3]F. Bisio, R. Moroni, F. Buatier de Mongeot, M. Canepa, and L. Mattera, Appl. Phys. Lett. **89**, 52507 (2006).
[4]Q.-F. Zhan, S. Vandezande, K. Temst, and C. Van Haesendonck, New. J. Phys. **11**, 63003 (2009).
[5]W. C. Lin, S. S. Wong, P. C. Huang, C. B. Wu, B. R. Xu, C. T. Chiang, H. Y. Yen, and M.-T. Lin, Appl. Phys. Lett. **89**, 153111 (2006).
[6]Y. Shim, V. Borovikov, and J. G. Amar, Phys. Rev. B **77**, 235423 (2008).
[7]Y. Shim and J. G. Amar, Phys. Rev. Lett. **98**, 46103 (2007).
[8]S. van DDijken, L. C. Jorritsma, and B. Poelsema, Phys. Rev. Lett. **82**, 4038 (1999).
[9]A. Amassian, K. Kaminska, M. Suzuki, L. Martinu, and K. Robbie, Appl. Phys. Lett. **91**, 173114 (2007).
[10]Q.-F. Zhan, S. Vandezande, K. Temst, and C. Van Haesendonck, Phys. Rev. B **80**, 94416 (2009).
[11]Y.-P. Fang, W. He, H.-L. Liu, Q.-F. Zhan, H.-F. Du, Q. Wu, H.-T. Yang, X.-Q. Zhang, and Z.-H. Cheng, Appl. Phys. Lett. **97**, 22507 (2010).
[12]Q.-F. Zhan, C. Van Haesendonck, S. Vandezande, and K. Temst, Appl. Phys. Lett. **94**, 42504 (2009).
[13]M. M. Hawkeye and M. J. Brett, J. Vac. Sci. Technol. A **25**, 1317 (2007).
[14]J. L. Bubendorff, G. Garreau, S. Zabrocki, D. Berling, R. Jaafar, S. Hajjar, A. Mehdaoui, and C. Pirri, Surf. Sci. **603**, 373 (2009).
[15]V. Madurga, J. Vergara, and C. Favieres, J. Magn. Magn. Mater. **272**, 1681 (2004).
[16]J. L. Bubendorff, S. Zabrocki, G. Garreau, S. Hajjar, R. Jaafar, D. Berling, A. Mehdaoui, C. Pirri, and G. Gewinner, Europhys. Lett. **75**, 119 (2006).
[17]G. A. Wurtz, W. Hendren, R. Pollard, R. Atkinson, L. Le Guyader, A. Kirilyuk, Th. Rasing, I. I. Smolyaninov, and A. V. Zayats, New J. Phys. **10**, 105012 (2008).
[18]M. Pasturel, M. Slaman, H. Schreuders, J. H. Rector, D. M. Borsa, B. Dam, and R. Griessen, J. Appl. Phys. **100**, 23515 (2006).
[19]Y. H. Liou, W. F. Pong, M.-H. Tsai, K. H. Chang, H. H. Hseih, Y. K. Chang, F. Z. Chien, P. K. Tseng, J. F. Lee, Y. Liou, and J. C. A. Huang, Phys. Rev. B **62**, 9616 (2000).
[20]S. D'Addato, L. Marassi, P. Luches, G. C. Gazzadi, L. Pasquali, R. Verucchi, P. Finetti, and S. Nannarone, Surf. Sci. **487**, 258 (2001).
[21]C.-W. Pao, C.-T. Wu, H.-M. Tsai, Y.-S. Liu, C.-L. Chang, W. F. Pong, J.-W. Chiou, C.-W. Chen, M.-S. Hu, M.-W. Chu, L.-C. Chen, C.-H. Chen, K.-H. Chen, S.-B. Wang, S.-J. Chang, M.-H. Tsai, H.-J. Lin, J.-F. Lee, and J.-H. Guo, Phys. Rev. B **84**, 165412 (2011).
[22]R. A. Gordon, E. D. Crozier, D.-T. Jiang, T. L. Monchesky, and B. Heinrich, Phys. Rev. B **62**, 2151 (2000).
[23]S.-J. An, W. I.Park, G.-C. Yi, and S. Cho, Appl. Phys. A **74**, 509 (2002).
[24]E. E. Fullerton, D. Stoeffler, K. Ounadjela, B. Heinrich, Z. Celinski, and J. A. C. Bland, Phys. Rev. B **51**, 6364 (1995).
[25]W. C. Lin, F. Y. Lo, Y. Y. Huang, C. H. Wang, and M. Y. Chern, J. Appl. Phys. **110**, 83911 (2011).
[26]Y.-F. Han, D. Kumar, and D. W. Goodman, J. Catal. **230**, 353 (2005).
[27]Z. Łodziana and J. K. Nørskov, J. Chem. Phys. **115**, 11261 (2001).
[28]Y. S. Dedkov and M. Fonin, Appl. Surf. Sci. **253**, 3860 (2007).
[29]E. A. Soares, M. A. Van Hove, C. F. Walters, and K. F. McCarty, Phys. Rev. B **65**, 195405 (2002).
[30]Yu. Shiratsuchi, Y. Endo, and M. Yamamoto, Sci. Technol. Adv. Mater. **5**, 73 (2004).
[31]J. J. Rehr, J. Mustre de Leon, S. I. Zabinsky, and R. C. Albers, J. Am. Chem. Soc. **113**, 5135 (1991).
[32]A. I. Frenkel, E. A. Stern, M. Qian, and M. Newville, Phys. Rev. B **48**, 12449 (1993).
[33]C. T. Campbell, Surf. Sci. Rep. **27**, 1 (1997).
[34]F. Bisio, A. Toma, R. Moroni, R. Pasero, F. Buatier de Mongeot, C. Boragno, M. Canepa, U. Valbusa, and L. Mattera Phys. Rev. B **75**, 54407 (2007).
[35]M. T. Umlor, Appl. Phys. Lett. **87**, 82505 (2005).
[36]F. Bisio, R. Moroni, A. Chincarini, M. Canepa, and L. Mattera, J. Appl. Phys. **104**, 33905 (2008).
[37]H. P. Oepen, Y. T. Millev, H. F. Ding, S. Pütter, and J. Kirschner, Phys. Rev. B **61**, 9506 (2000).